Preparation of High Modulus Polyethylene Sheet By the Roller-Drawing Method

AKIRA KAITO, KAZUO NAKAYAMA, and HISAAKI KANETSUNA,
Research Institute for Polymers and Textiles, 1-1-4, Yatabe-Higashi, Tsukuba, Ibaraki 305, Japan

Synopsis

The high density polyethylene (HDPE) sheets were drawn through a pair of heated rollers. The process, referred to as roller drawing, was found to be useful for producing high modulus and high strength HDPE sheets. The higher draw ratio could be obtained for the HDPE sheet with lower molecular weight and narrower molecular weight distribution. The Young's modulus and the breaking strength reached 43 GPa and 0.67 GPa, respectively, at the highest draw ratio. The measurements of wide-angle X-ray diffraction (WAXD) pole figures revealed that the crystallographic *a*-, *b*-, and *c*-axes were oriented to the normal direction (ND), the traverse direction (TD), and the drawing direction (DD), respectively. The small-angle X-ray scattering (SAXS) of the roller-drawn HDPE sheets with draw ratio higher than 7 exhibited two intensity maxima on the meridian, suggesting the presence of the two-phase structure in which crystalline and amorphous regions are stacked alternately along DD. The relationship between mechanical properties and microstructure was discussed on the basis of the concept of the formation of amorphous tie molecules in the interfibrillar and intercrystallite regions.

INTRODUCTION

Solid-state deformation of thermoplastic polymers has been extensively studied aiming at producing high modulus and high strength polymeric materials. The various forming methods, such as tensile drawing,[1] rolling,[2] hydrostatic extrusion,[3,4] and solid-state extrusion[5] have been reported over the last decade. The tensile drawing was shown to produce high modulus and high strength tapes and fibers.[1] However, the major limitation of the tensile drawing is the difficulty in producing samples with large cross section. The rolling has advantage of being applicable to the thick polymer sheets. However, on removal of the roller pressure, the elastic energy stored in the amorphous region of the material causes the thickness recovery, which lowers the thickness reduction ratio. The rolled polymers are generally not so stiff as the highly drawn polymer sheets.

Recently Ward and his co-workers[6-9] reported die drawing, a process for the production of high modulus thermoplastic rods with large diameter. However, the die-drawing process applicable to polymer sheets has not been reported yet.

In this work, we attempt to draw high density polyethylene (HDPE) sheets through a pair of heated rollers. The process, hereafter called roller drawing, has the following advantages over conventional tensile drawing and rolling of polymer sheets.

(i) As thickness recovery is restricted, high draw ratio is achieved. Ac-

Journal of Applied Polymer Science, Vol. 30, 1241–1255 (1985)

CCC 0021-8995/85/ 031241-15$04.00

cordingly, the roller drawing is useful for the preparation of high modulus and high strength polymer sheets.

(ii) The roller drawing has possibility of being applicable to thick polymer sheets and of developement into a continuous process.

(iii) The draw ratio can be controlled by both roller spacing and draw velocity.

(iv) The apparatus for the roller drawing is relatively simple. The mechanical properties, the molecular orientation, and the microstructure of the roller-drawn HDPE sheets are investigated.

EXPERIMENTAL

Sample Preparation

The samples used in this work were two grades of HDPE, Hizex 2200 J ($\overline{M}_w$ = 61000, $\overline{M}_n$ = 8300) and Hizex 5000 B ($\overline{M}_w$ = 160,000, $\overline{M}_n$ = 11,000) produced by Mitsui Petrochemical Co., Ltd. Sheets 0.8–0.9 mm thick were prepared by compression-molding the pellets of Hizex 2200 J at 200–220°C under a pressure of 4 MPa, while 5000 B sheets 1 mm thick were obtained from commercial source. The 2200 J and 5000 B sheets were cut into strips 20 mm wide and 30 mm wide, respectively, which were used for the roller-drawing experiment.

The roller drawing was carried out using an apparatus schematically shown in Figure 1. A pair of heated rollers with a diameter of 50 mm were attached to the upper side of the crosshead of a tensile testing machine, tensilon UTM-10T (Toyo Baldwin Co., Ltd.). An original sheet, preheated between hot plates, was drawn through the rollers at a constant draw velocity, v_d, of 10–500 mm/min by lowering the crosshead of the tensile testing machine. The draw load was measured by a load cell mounted at the top of the tensile testing machine. The roller drawing of the 2200 J

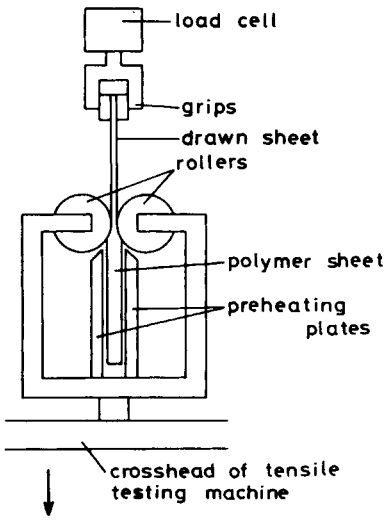

Fig. 1. Apparatus for the roller-drawing of polymer sheets.

sheet was performed at roller temperature, T_r of 75°C and 100°C, and T_r was set at 100°C and 120°C for the 5000 B sheet.

Characterization

Tensile tests were carried out at 23 ± 1°C and a relative humidity of 50 ± 2% using a tensile testing machine, tensilon UTM-III-100 (Toyo Baldwin Co., Ltd.), with a gauge length of 12.5 mm and a tensile rate of 4 mm/min.

Wide-angle X-ray diffraction (WAXD) pole figures were measured by employing both reflection and transmission techniques. The X-ray intensity was corrected for background and absorption. The degree of orientation of the crystallographic *c*-axis was calculated from WAXD azimuthal scanning data for 002 reflection, using Hermans-type orientation function.[10]

The crystallite sizes were calculated from the integrated line width using a Scherrer equation,[11] after the WAXD intensity profiles were corrected for Kα doublet and instrumental broadenings using reflections of silica.

The 200 and 020 pole figures and crystallite sizes were measured with Ni-filtered Cu Kα radiation (40 kV, 25 mA) produced by a Geiger Flex XGC-20 (Rigaku Denki Co., Ltd.), while Zr-filtered Mo Kα radiation (40 kV, 40 mA) was used for the measurements of 002 pole figure.

Small-angle X-ray scattering (SAXS) patterns were taken with a vacuum camera using Ni-filtered Cu Kα radiation (40 kV, 100 mA) produced by a Rota Flex RU-200 (Rigaku Denki Co., Ltd.). In order to evaluate the long period, the SAXS intensity distribution was measured using a scintillation counter.

Birefringence was measured by the retardation method using a polarized microscope equipped with a Berek compensator. The degree of orientation in the amorphous region was estimated from birefringence using an equation proposed by Stein.[12] The values of 0.0585 and 0.12 were used for the intrinsic birefringence of completely oriented crystalline and amorphous regions, respectively.[13]

The melting behavior of the samples was examined at a constant heating rate of 5°C/min with a Perkin-Elmer DSC-2 Differential Scanning Calorimeter calibrated with a melt transition of Indium (156.5°C).

Density was measured using an ethanol–water density gradient column at 25°C. The degree of crystallinity, the volume fraction of crystalline phase, was calculated assuming the densities of the crystalline and amorphous phases to be 0.999 g/cm^3 and 0.8525 g/cm^3, respectively.[14,15]

RESULTS AND DISCUSSION

Appearance

The roller drawing produced HDPE sheets with smooth surfaces and uniform thickness. The 5000 B sheets became transparent by the roller drawing, while the roller-drawn 2200 J sheets were translucent or opaque.

The width of the sheets contracted by the roller drawing. The degree of width contraction depended upon draw velocity and sample grade, but was not so sensitive to drawing temperature and deformation ratio. The degrees

of width contraction of 2200 J and 5000 B sheets were 25–35% and 5–10%, respectively, in the low draw velocity range (v_d = 10–50 mm/min). The degree of width contraction of 5000 B sheets increased with increasing draw velocity and reached 20–27% at v_d = 500 mm/min.

Relationship Between Drawing Stress, Deformation Ratio, and Roller Spacing

Drawing stress, draw ratio, and the ratio of sheet thickness after and before roller drawing, t/t_0, are plotted in Figure 2 as functions of the ratio of roller spacing to the original sheet thickness, t_r/t_0. Here, drawing stress is determined by the ratio of draw load to cross sectional area of the original sheets, and the draw ratio λ is defined by the ratio of length after and before roller-drawing.

The 2200 J sheets fractured between rollers when they were drawn at v_d > 50 mm/min. The 5000 B sheets could be drawn at v_d up to 500 mm/min, but the roller drawing at v_d = 500 mm/min was possible only for wide roller openings ($t_r/t_0 \simeq 0.4$).

The roller drawing consists of two deformation processes: isothermal thickness reduction between rollers and nonisothermal tensile flow in the post roller zone. The roller-drawn 2200 J sheets were much thinner than roller spacing ($t/t_0 << t_r/t_0$), suggesting that the 2200 J sheets were stretched to a large extent in the post-roller zone. On the other hand, the

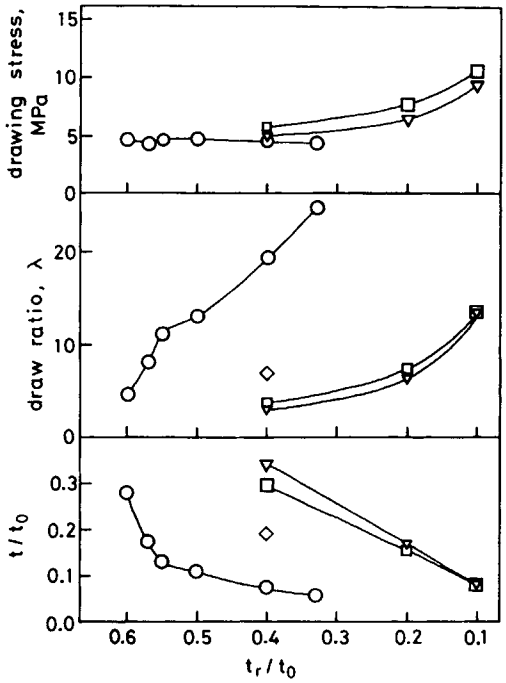

Fig. 2. Drawing stress, draw ratio (λ), and the ratio of sheet thickness after and before roller-drawing (t/t_0) vs. the ratio of roller spacing to original sheet thickness (t_r/t_0): (○) 2200 J; roller temperature, T_r = 100°C; draw velocity, v_d = 50 mm/min; (□) 5000 B, T_r = 100°C, v_d = 50 mm/min; (▽) 5000 B, T_r = 100°C, v_d = 10 mm/min; (◇) 5000 B, T_r = 100°C, v_d = 500 mm/min.

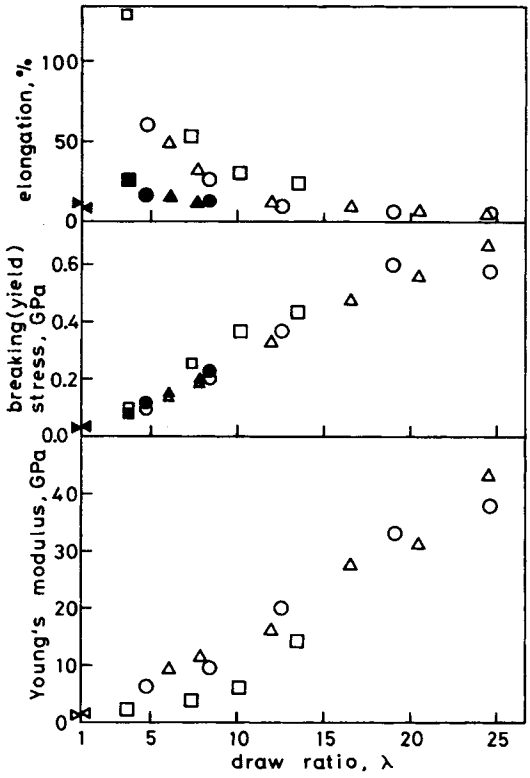

Fig. 3. Mechanical properties vs. draw ratio (λ): (△,▲) 2200 J, T_r = 75°C; (○,●) 2200 J, T_r = 100°C; (□,■) 5000 B, T_r = 100°C; (◁,◀) original 2200 J sheet; (▷,▶) original 5000 B sheet: open symbols represent elongation at break, breaking strength, and Young's modulus, and filled symbols stand for yield elongation and yield strength.

roller-drawn 5000 B sheets were a little thinner than roller spacing, and their thickness approached roller spacing ($t/t_0 \approx t_r/t_0$) as roller spacing was narrowed. The thickness reduction between rollers was the main deformation process for the heavy roller drawing of the 5000 B sheets.

In the case of hot rolling, the thickness of sheets elastically recovered in part after they passed through rollers.[16] However, thickness recovery was not observed in the roller-drawing of HDPE.

The draw ratio increased with decreasing roller spacing and increasing draw velocity. The 2200 J sheets could be drawn up to $\lambda \approx 25$ at T_r = 75°C and 100°C.

The drawing stress for the 5000 B sheets increased with decreasing roller spacing. At a given roller spacing, higher speed drawing required higher drawing stress. The drawing stress for the 2200 J sheets was lower than that for the 5000 B sheets and was not much affected by roller spacing.

Tensile Properties

The tensile properties of the roller-drawn HDPE sheets are shown in Figure 3 as functions of draw ratio. In the case of the original sheets and the lightly drawn sheets ($\lambda < 5$ for the 5000 B sheets and $\lambda < 9$ for the 2200 J sheets), a yield point was observed in the stress–strain curve. On

TABLE I
Tensile Properties of the HDPE Sheets Roller-Drawn to the Maximum Draw Ratio (λ_{max})

Grade	T_r (°C)	λ_{max}	Young's modulus (GPa)	Tensile strength (GPa)	Elongation at break (%)
2200 J	75	24.5	43	0.67	4.6
2200 J	100	24.7	38	0.58	5.0
5000 B	100	13.8	16	0.47	18.0
5000 B	120	14.3	11	0.40	5.6

the other hand, the sheets with higher draw ratio uniformly deformed without showing a yield point during tensile test. The breaking strength, the yield strength, and the Young's modulus increased with increasing draw ratio. The elongation at break decreased with increasing draw ratio rapidly at lower draw ratio and gradually at higher draw ratio. At the same draw ratio, the Young's modulus of the 5000 B sheets was lower than that of the 2200 J sheets.

The tensile properties of the HDPE sheets roller-drawn to the maximum draw ratio, λ_{max} are shown in Table I. The Young's modulus as high as 38–43 GPa was attained by roller drawing the 2200 J sheet at T_r = 75°C and 100°C. The 5000 B sheets could be roller-drawn to $\lambda_{max} \approx 14$ at both T_r = 100°C and 120°C, and the Young's modulus at λ_{max} decreased as T_r rose.

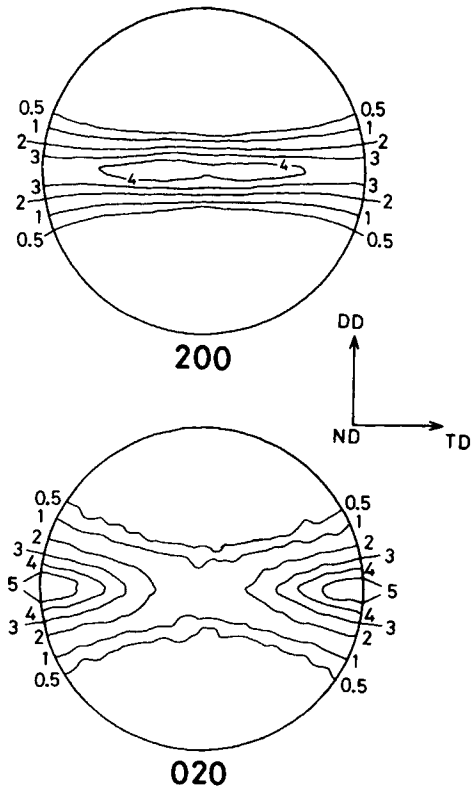

Fig. 4. 200 and 020 pole figures of the roller-drawn 2200 J sheet (T_r = 100°C, λ = 4.8).

Pole Figures

The 200 and 020 pole figures measured for the roller-drawn 2200 J sheets (T_r = 100°C) are shown in Figures 4 and 5. The principal axes of the sheets are labeled DD (drawing direction), TD (traverse direction), and ND (normal direction). The contour lines were drawn in units of the intensity of random sample. The 200 and 020 poles were distributed in the ND–TD plane, and showed maxima at ND and TD, respectively. The 200 and 020 poles of the highly drawn sample (λ = 24.7) were more sharply distributed than those of the lightly drawn sheet (λ = 4.8).

The 200 and 020 pole figures of the 5000 B sheets (T_r = 100°C) are presented in Figures 6 and 7. Although the pole figures of the 5000 B sheet of λ = 3.7 bore a resemblance to those of the 2200 J sheet of λ = 4.8, the former showed higher degree of crystal orientation than the latter. In the 5000 B sheet of λ = 13.8, the 200 pole showed a small maximum at 56° from ND to TD, in addition to the large maximum at ND. A small maximum was also observed at 59° from TD to ND in the 020 pole figure. The pole maxima caused by (310) and (110) twinnings should be located about 54° and 68° from the main maximum, respectively.[17] Therefore, (310) and (110) twinnings are considered to be produced by the heavy roller drawing of the 5000 B sheet.

Figure 8 shows draw ratio dependence of the 002 pole figures of the 5000 B sheets measured at Bragg angle, 2θ = 32.4° (Mo Kα radiation). The

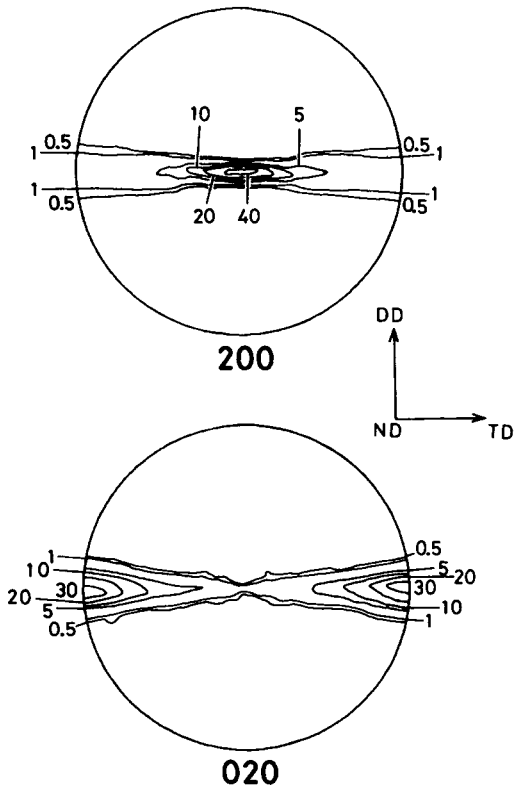

Fig. 5. 200 and 020 pole figures of the roller-drawn 2200 J sheet (T_r = 100°C, λ = 24.7).

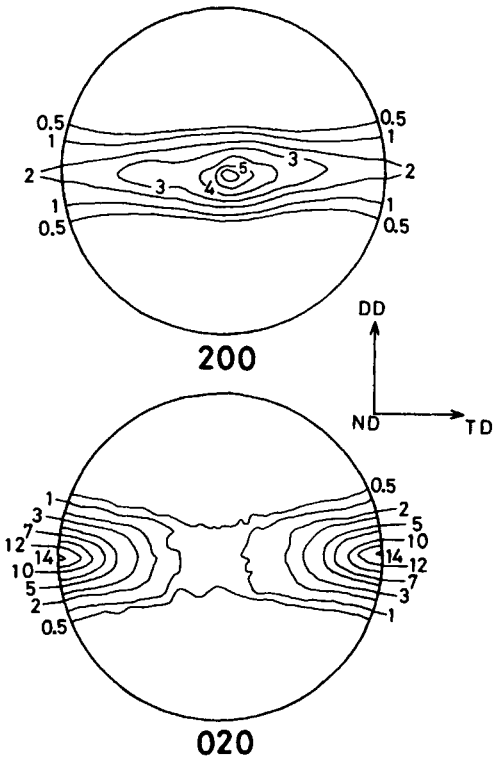

Fig. 6. 200 and 020 pole figures of the roller-drawn 5000 B sheet (T_r = 100°C, λ = 3.7).

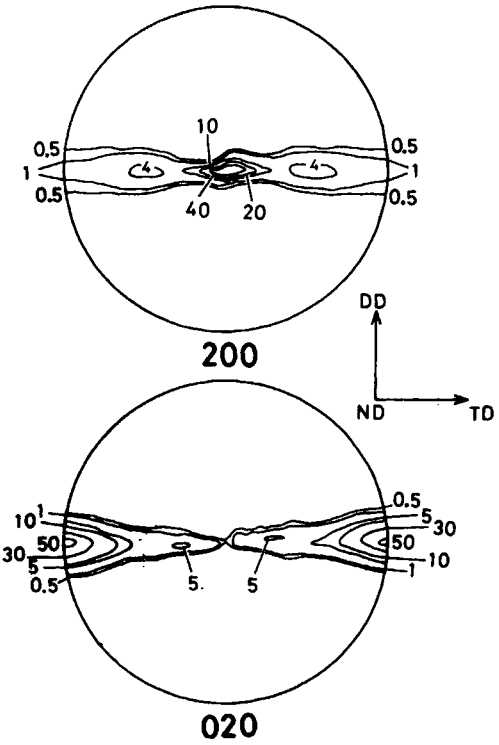

Fig. 7. 200 and 020 pole figures of the roller-drawn 5000 B sheet (T_r = 100°C, λ = 13.8).

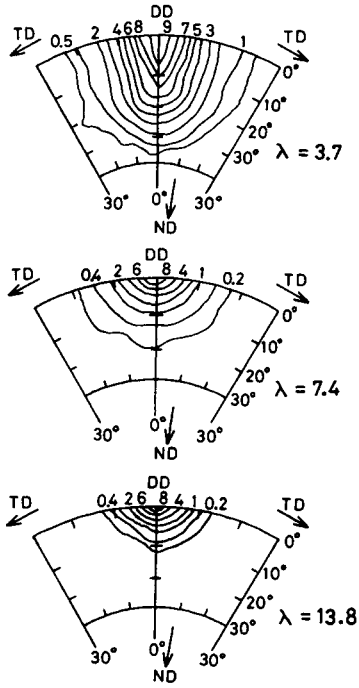

Fig. 8. Draw ratio dependence of the 002 pole figure of the roller-drawn 5000 B sheet (T_r = 100°C).

intensity contour labelled 1, 2, · · ·, and 9 represents 10, 20, · · ·, and 90% of the maximum intensity, respectively. The 002 pole figure was accompanied by the poles of 231, 421, 520, 511, and 430 reflections which lie at $31.7° < 2\theta < 33.5°$. However, they were separated from the 002 pole maximum by more than 59° in the oriented samples, and were not shown here. At lowest draw ratio ($\lambda = 3.7$), the 002 pole was spread to ND rather than to TD, suggesting that some of the molecular chains tended to be inclined from DD in the DD–ND plane. On the other hand, in the highly drawn 5000 B sheets ($\lambda \geq 7.4$), the 002 pole was almost uniaxially distributed to DD.

We also measured the 002 pole figures of the roller-drawn 2200 J sheets. The *c*-axis of the 2200 J sheets of $\lambda \geq 8.4$ was in uniaxial alignment to DD.

Birefringence and Degree of Orientation

The value of birefringence increased with increasing draw ratio and exceeded the intrinsic birefringence of completely oriented crystalline phase at $\lambda \simeq 25$. The intrinsic birefringence of the amorphous region may be greater than that of the crystalline phase because of the internal field effects.[18]

The 002 pole figure showed that the c-axis of the roller-drawn HDPE sheets of $\lambda \geq 7.4$ uniaxially aligned to DD (Fig. 8). As the difference of the principal refractive indices of polyethylene crystal, n_a and n_b is small, the (100) plane orientation in the sheet plane does not have an important effects on the anisotropy of the refractive indices. The experimental values of birefringence Δn_{DD-ND} was in agreement with that of Δn_{DD-TD}, within a limit

of experimental error ($\approx 10^{-3}$), suggesting that the average anisotropy in the roller-drawn HDPE sheets were almost uniaxial. On the basis of these results, the amorphous molecular chains were assumed to be uniaxially oriented to DD similarly to the crystal c-axis. The degree of amorphous orientation was calculated using $\Delta n_{cr} = 0.0585$ and $\Delta n_{am} = 0.12$ for the intrinsic birefringence of completely oriented crystalline and amorphous phases, respectively, which were recently reported for polyethylene samples with fibrillar morphology.[13]

The degree of orientation of the c-axis, f_c, and the amorphous region, f_{am}, are shown in Figure 9. Although f_c reached a constant value of 0.96–0.97 at $\lambda > 10$, f_{am} monotonically increased with increasing draw ratio.

Small Angle X-ray Scattering

Figure 10 shows SAXS patterns of the roller-drawn 5000 B sheets with incident X-ray beam parallel to ND and TD (hereafter called ND-pattern and TD-pattern, respectively). At every draw ratio, the ND-pattern showed a two-point diagram on the meridian. The TD-pattern at $\lambda = 3.7$ was arc-shaped, suggesting that there are two kinds of lamellar structure; one in which lamellar normals are almost parallel to DD and another in which lamellar normals are 60–65° inclined from DD in the DD–ND plane. The TD-pattern at $\lambda \geq 7.4$ exhibited two streaks on the meridian. The two-phase structure, in which crystalline and amorphous regions are stacked alternately along DD, is presented in the 5000 B sheet of $\lambda \geq 7.4$. In the TD-pattern at higher draw ratio, we observed equatorial scattering arising from interfibrillar microvoids.

Figure 11 shows SAXS patterns of the roller-drawn 2200 J sheets. The TD-pattern at $\lambda = 4.8$ showed a complicated intensity distribution. The 2200 J sheets of $\lambda \geq 8.4$ showed two-point or two-streak SAXS diagrams, similarly to the 5000 B sheets.

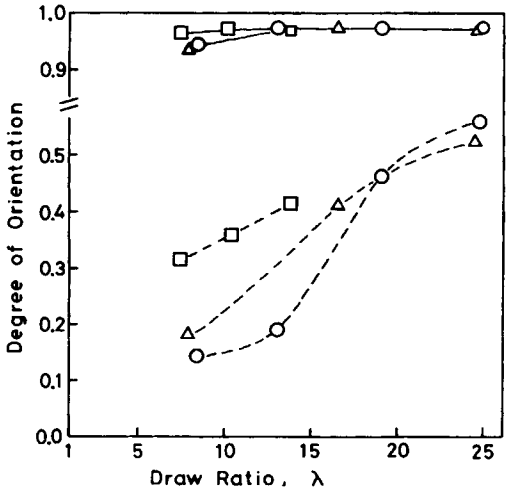

Fig. 9. Degree of orientation in crystalline (——) and amorphous (—) regions vs. draw ratio (λ): (△) 2200 J, $T_r = 75$°C; (○) 2200 J, $T_r = 100$°C; (□) 5000 B, $T_r = 100$°C.

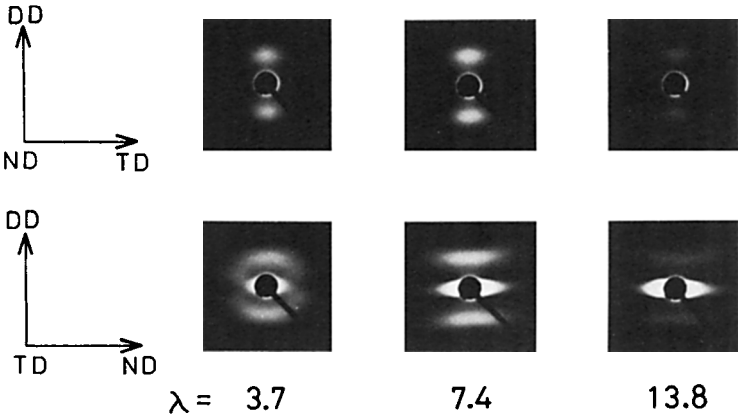

Fig. 10. SAXS patterns of the roller-drawn 5000 B sheets (T_r = 100°C).

The horizontal breadth of the meridional SAXS gives information on the lateral dimension of the periodic layer. According to Gerasimov et al.,[19] the meridional SAXS with broader horizontal breadth is originated from the periodic structure with smaller lateral dimension. The relationship between SAXS pattern and periodic structure for the roller-drawn HDPE sheets is schematically shown in Figure 12. The crystallites are arranged along TD with the molecular chains parallel to DD forming coherent crystalline layers in SAXS. Therefore, the two-point SAXS diagram was observed in the ND-pattern. On the other hand, the two-streak SAXS diagram in the TD pattern suggests the presence of fibrillar structure in the DD–ND plane.

Crystallite Size and Long Period

Table II shows the crystallite size in the direction normal to the (200), (020), and (002) planes, D_{200}, D_{020}, and D_{002}, and the long period L is measured with incident X-ray beam parallel to ND. The values of D_{200} and D_{020} monotonically decreased with draw ratio, suggesting that the cleavage of crystallites occured in the (100) and (010) planes. The long period L decreased

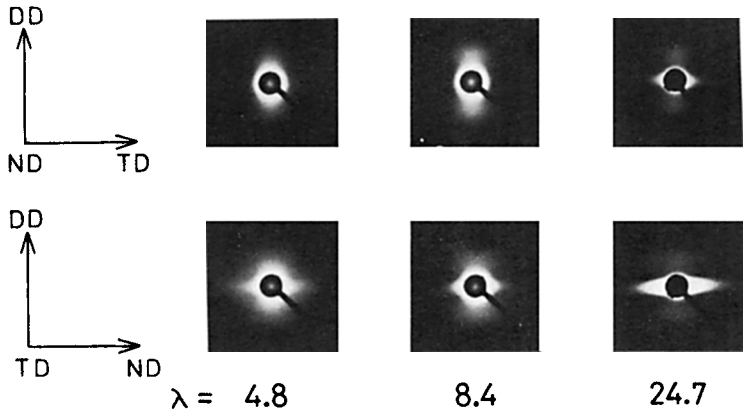

Fig. 11. SAXS patterns of the roller-drawn 2200 J sheets (T_r = 100°C).

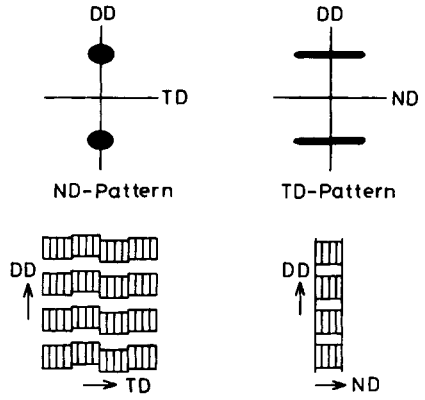

Fig. 12. Relationship between SAXS pattern and periodic structure for the roller-drawn HDPE sheets.

with increasing draw ratio in the lower draw ratio range and reached a constant value at higher draw ratio.

The crystallite sizes and the long period increased with the rise of roller temperature. At same draw ratio and roller temperature, the 5000 B sheet showed smaller crystallite sizes and long period than 2200 J sheet.

The degree of crystallinity was somewhat greater than the ratio of D_{002} to L. However, if one considers that the values of D_{002} and L have a wide distribution and that the c-axis and the lamellar normal are not sufficiently oriented to DD at lower draw ratio, the agreement between crystallinity and D_{002}/L is fairly good. This confirms that the basic structure of the roller-drawn HDPE sheets is a two-phase structure.

Wu et al.[20] also reported that the crystallinity of the ultradrawn polyethylene fibers was greater than the ratio of D_{002} to L. They explained the result by crystallization of interfibrillar and intercrystallite tie molecules.

On the other hand, Gibson et al.[21,22] reported that D_{002} increased sometimes more than twice with increasing draw ratio and exceeded the long

TABLE II
Crystallite Sizes (D_{200}, D_{020}, and D_{002}), Long Period (L), and Degree of Crystallinity (χ) of the Roller-Drawn HDPE Sheets

Grade	T_r (°C)	λ	D_{200} (nm)	D_{020} (nm)	D_{002} (nm)	L (nm)	χ (%)
2200 J	100	4.8	13.4	12.3	18.8	35.8	79.3
		8.4	12.4	11.2	18.5	31.2	78.2
		13.1	11.9	11.1	20.0	27.3	80.0
		19.1	12.2	11.2	21.1	27.7	80.6
		24.7	11.9	11.1	21.1	27.7	82.3
5000 B	100	3.7	11.9	13.1	15.9	25.2	68.2
		7.4	11.6	11.1	16.5	22.7	70.7
		10.2	11.1	11.1	17.0	22.8	72.1
		13.8	10.6	10.8	17.4	23.2	71.7
5000 B	120	4.9	15.3	14.2	19.2	34.1	74.2
		9.2	14.7	13.2	20.1	34.5	75.8
		14.3	13.4	12.6	19.5	29.7	76.1

period at higher draw ratio in hot drawn and hydrostatically extruded HDPE. They explained the large increase in D_{002} by the increase in the crystalline continuity in the c-axis direction. However, in the present work, D_{002} increased with draw ratio more gradually than the result of their works and never exceeded the long period. Although the reason for the difference is not clear, this may be possibly explained by the difference in processing procedure or processing condition.

Melting Behavior

The roller-drawn HDPE sheets showed a single melting peak on the DSC curve. The DSC peak melting temperature of the roller-drawn sheets is plotted in Figure 13 as a function of draw ratio. The peak melting temperature never exceeded 138°C, suggesting that the roller-drawn HDPE sheet does not contain an extended chain morphology as found in pressure-crystallized HDPE.[23] The peak melting temperature increased with increasing draw ratio. At the same draw ratio, the 2200 J sheet showed higher peak melting temperature than the 5000 B sheet.

The highly drawn 2200 J sheet ($\lambda = 24.7$) showed superheating effects. The peak melting temperature increased by 3.9°C with increasing heating rate from 1.25°C/min to 40°C/min. The increase in the peak melting temperature with draw ratio may be due to the increase in constraints on the amorphous region.[24]

Molecular Weight Effects

As the 5000 B has a higher $\overline{M}_w$ value and broader molecular weight distribution than the 2200 J, the 5000 B contains a larger amount of high molecular weight fraction. In the 5000 B, the entanglements of long molecular chains tend to form a network superstructure.[25] The network superstructure plays an important role in the deformation mechanism and

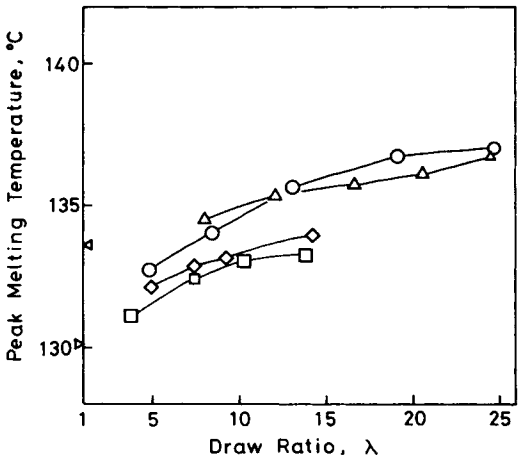

Fig. 13. Peak melting temperature vs. draw ratio (λ): (△) 2200 J, T_r = 75°C; (○) 2200 J, T_r = 100°C; (□) 5000 B, T_r = 100°C; (◇) 5000 B, T_r = 120°C; (◁) original 2200 J sheet; (▷) original 5000 B sheet.

would enhance a resistance to plastic deformation. Therefore, the non-isothermal plastic flow in the post-roller zone was restricted in the roller drawing of the 5000 B sheet.

Hay and Keller[2] reported the presence of twinned lattice in rolled polyethylene. On removal of roller pressure, the elastic energy stored in the amorphous region generates the compressive forces along traverse direction, which induce twinnings of lattice along (310) and (110) planes. The roller-drawn 5000 B sheet of $\lambda = 13.8$ showed a small pole maxima due to the (310) and (110) lattice twinnings in the 200 and 020 pole figures, while no lattice twinning was observed for the roller-drawn 2200 J sheets. As crystallization is restricted by the chain entanglements, the 5000 B sheet contains larger amount of amorphous materials than the 2200 J sheet. In the case of the 5000 B sheet of $\lambda = 13.8$, the elastic energy stored in the entangled amorphous chains is enough to cause lattice twinnings. On the other hand, for the 2200 J sheets with higher crystallinity, the elastic energy is not sufficient for inducing lattice twinnings.

Relationship between Young's Modulus and Microstructure

The degree of crystal orientation and the crystallite sizes are not much changed with draw ratio at higher draw ratio ($\lambda > 10$). The Young's modulus and the breaking strength continued to increase at $\lambda > 10$. Hence, the increase in the mechanical properties $\lambda > 10$ may be ascribable to the changes in the intercrystallite and interfibrillar regions. According to the deformation mechanism proposed by Peterlin,[26,27] amorphous taut tie molecules are formed in the interfibrillar and intercrystallite regions. The tie molecules increase in number and tautness with increasing draw ratio. Several authors[20–22,28] reported the possibility of crystallization of the tie molecules into crystalline bridges. The formation of the tie molecules would increase the orientation of amorphous chains, as observed in this work. As number of tie molecules increases, crystallites would exert configurational constraint on amorphous regions and restrict the mobility of amorphous chains.

Wu et al.[20] reported that the intensity of the meridional SAXS correlated well with the strength of the HDPE fibers. We also observed that the SAXS intensity of the roller-drawn HDPE sheets decreased with increasing draw ratio. The interfibrillar and intercrystallite links increase the density of interfibrillar and intercrystallite regions, which decreases the intensity of the meridional SAXS.

Therefore, the increase in the mechanical properties above $\lambda = 10$ may be originated from the formation of the interfibrillar and intercrystallite links and the increase in amorphous orientation.

CONCLUSION

The roller drawing was found to be a useful procedure for producing high modulus and high strength HDPE sheets. The thickness recovery, which is incidental to hot rolling of polymer sheets, was not observed in the roller drawing of the HDPE sheets. The 2200 J sheet with lower molecular weight and narrower molecular weight distribution was considerably stretched

after passing through rollers, resulting in the achievement of higher Young's modulus.

The measurements of WAXD pole figures revealed that the crystallographic *a*-, *b*-, and *c*-axes became oriented to ND, TD, and DD, respectively. The (310) and (110) twinnings were observed only for the 5000 B sheet drawn to the maximum draw ratio. The SAXS of the roller-drawn HDPE sheets of $\lambda \geq 7.4$ revealed the presence of the two-phase structure in which crystalline and amorphous regions are stacked alternately along DD.

With increasing draw ratio, the SAXS intensity decreased, the degree of amorphous orientation increased, and the DSC melting peak shifted to higher temperature. These changes are considered to be related to the formation of tie molecules in the interfibrillar and intercrystallite regions.

References

1. G. Capaccio, T. A. Crompton, and I. M. Ward, *J. Polym. Sci., Polym. Phys. Ed.*, **14**, 1641 (1976).
2. I. L. Hay and A. Keller, *J. Mater. Sci.*, **1**, 41 (1966).
3. K. Nakayama and H. Kanetsuna, *J. Mater. Sci.*, **10**, 1105 (1975).
4. A. G. Gibson and I. M. Ward, *J. Polym. Sci., Polym. Phys. Ed.*, **16**, 2015 (1978).
5. W. G. Perkins, N. J. Capiati, and R. S. Porter, *Polym. Eng. Sci.*, **16**, 200 (1976).
6. P. D. Coates and I. M. Ward, *Polymer*, **20**, 1553 (1979).
7. A. G. Gibson and I. M. Ward, *Polym. Eng. Sci.*, **20**, 1229 (1980).
8. A. G. Gibson and I. M. Ward, *J. Mater. Sci.*, **15**, 979 (1980).
9. P. S. Hope, A. Richardson, and I. M. Ward, *J. Appl. Polym. Sci.*, **26**, 2879 (1981).
10. P. H. Hermans, *Physics and Chemistry of Cellulose Fibres*, Elsevier, Amsterdam, 1949.
11. P. Scherrer, *Gött. Nachr.*, **2**, 98 (1918).
12. R. S. Stein, *J. Polym. Sci.*, **31**, 327 (1958).
13. A. R. Wedgewood and J. C. Seferis, *Polym. Eng. Sci.*, **24**, 328 (1984).
14. P. R. Swan, *J. Polym. Sci.*, **56**, 403, (1962).
15. M. G. Gubler and A. J. Kovacs, *J. Polym. Sci.*, **34**, 551 (1959).
16. D. P. Pope and A. Keller, *J. Mater. Sci.*, **9**, 920 (1974).
17. O. Yoda and I. Kuriyama, *J. Polym. Sci., Polym. Phys. Ed.*, **15**, 773 (1977).
18. M. Pietralla, H.-P. Grossmann, and J. K. Krüger, *J. Polym. Sci., Polym. Phys. Ed.*, **20**, 1193 (1982).
19. V. I. Gerasimov, Ya. V. Genin, and D. Ya. Tsvankin, *J. Polym. Sci., Polym. Phys. Ed.*, **12**, 2035 (1974).
20. W. Wu, P. G. Simpson, and W. B. Black, *J. Polym. Sci., Polym. Phys. Ed.*, **18**, 751 (1980).
21. A. G. Gibson, G. R. Davies, and I. M. Ward, *Polymer*, **19**, 683 (1978).
22. A. G. Gibson, G. R. Davies, and I. M. Ward, *Polym. Eng. Sci.*, **20**, 941 (1980).
23. T. Arakawa and B. Wunderlich, *J. Polym. Sci., C*, **16**, 563 (1967).
24. H. G. Zachmann, *Kolloid Z. Z. Polym.*, **206**, 25 (1965).
25. G. Capaccio and I. M. Ward, *Polymer*, **16**, 239 (1975).
26. A. Peterlin, *J. Polym. Sci., A-2*, **7**, 1151 (1969).
27. A. Peterlin, *J. Mater. Sci.*, **6**, 490 (1971).
28. A. Peterlin, *Polym. Eng. Sci.*, **18**, 488 (1978).

Received February 6, 1984
Accepted July 16, 1984